Optics Letters

Terahertz nonlinear index extraction via full-phase analysis

Kareem J. Garriga Francis, ⓘ Mervin Lim Pac Chong, Yiwen E, ⓘ and X.-C. Zhang*

The Institute of Optics, University of Rochester, Rochester, New York 14627, USA
*Corresponding author: xi-cheng.zhang@rochester.edu

We experimentally show the spectrally averaged nonlinear refractive index and absorption coefficient for liquid water, water vapor, α-pinene, and Si using a full-phase analysis in the terahertz regime through a standard time-domain spectrometer. Our results confirm that the nonlinear index of refraction of the liquid samples in this regime exceeds the near-infrared optical nonlinear index by six orders of magnitude. In the case of liquid water and water vapor at atmospheric pressure, we find a nonlinear index of 7.8×10^{-10} cm^2/W and 6×10^{-11} cm^2/W, respectively, which are both much larger than expected. © 2020 Optical Society of America

As more energetic sources of terahertz (THz) radiation are made available, there is a growing interest in understanding nonlinear effects in this elusive spectral region [1–3]. Recent investigations employing Z-scan techniques have shown that some materials exhibit nonlinear indices that are nearly six orders of magnitude larger than their optical counterparts [4]. Given the results found via the Z-scan method, in the specific case of analyzing the nonlinearity of liquid water, a THz peak electric field strength exceeding 3 MV/cm is enough to modify the refractive index by one order of magnitude. This change is enough to alter focusing and change expected results from spectroscopy while the wave maintains its non-ionizing properties, leading to several interesting nonlinear phenomena such as the possibility of enacting filamentation without plasma formation or elucidating nonlinear processes without the onset of optical breakdown. As such, it becomes apparent why probing nonlinearities in the THz regime is very exciting. Unfortunately, for Z-scan to be used effectively, the beam spatial mode (M^2) must be well known, and the source cannot be single-cycle [5]. Such constraints are not trivially solved in the optical regime and are even more cumbersome in the THz regime, where the sources are broadband and spatiotemporal focusing issues are abundant. In order to mediate mode issues in the optical regime, full-phase analysis experiments have been conducted using second-harmonic frequency-resolved optical gating (SHG FROG) and pulse reconstruction yielding much more accurate values for the nonlinear index of refraction than Z-scan techniques [5].

In this Letter, we show experimentally obtained values for the modification of the dielectric constants due to nonlinearity of liquid water, α-pinene, and Si. Given that THz time-domain spectroscopy (TDS) allows for the extraction of the phase of a captured signal, a full-phase analysis is instead conducted to extract nonlinear index n_2 and nonlinear absorption α_2. Our results show that material nonlinearities can be characterized directly with conventional THz-TDS systems. When spectrally averaged, the index of refraction indeed matches values previously obtained in Z-scan experiments. Moreover, improvements on the technique and the detection system would allow for spectrally resolved values of the Kerr coefficients. Similar experiments have been conducted in the optical regime using SHG FROG and pulse reconstruction yielding much more accurate values for the nonlinear index of refraction than Z-scan techniques [5].

All samples (liquid water, α-pinene, and Si) are evaluated via a THz-TDS system based on a two-color air-plasma source [6,7]. An amplified laser capable of providing 3 mJ, 800 nm, < 50 fs pulses at a 1 kHz repetition rate is used for the experiment. The laser is split into a pump–probe configuration with 2 mJ reserved for the pump beam. The resulting THz radiation is collected and guided to a conventional free-space electro-optic (EO) sampling setup [8] and controlled with a variable attenuator placed along the path of the pump beam. The THz peak electric field is measured at the sample position with EO sampling prior to measuring the samples. The peak electric field strength can be tuned between 10 kV/cm to 230 kV/cm, approximately corresponding to peak intensities of 0.3 and 140 MW/cm^2, respectively. Although the plasma source is essentially different, and its position moves slightly when the optical pump energy is varied, these effects are accounted for in the computation by recording signals as system references. Lastly, a knife-edge test is done to verify that the THz focal spot size leads to a Rayleigh range ($\sim$ 2 cm) that is larger than the sample thickness ($\sim$ 2 mm).

The sample cells are fabricated with a three-dimensional (3D) printer using natural white polylactic acid (PLA) material with a 100% infill and 0.06 mm layer height. The cells are treated as three-layer structures where 2-mm-thick α-pinene and 350-μm-thick water films are studied, respectively. In order to check for the validity of the analysis, Si is treated as a three-layer structure where two flat 500-μm-thick pieces of PLA sandwich

an 800-µm-thick Si wafer rather than as a single-layer structure. We choose samples that are known to be non-centrosymmetric, and whose responses have been previously characterized with Z-scan methods in order to compare with our full-phase analysis method. In the specific case of α-pinene, this liquid is chosen because it is a non-polar liquid, and it shows promise toward the development of THz liquid lasers.

In our full-phase analysis, we extract the index and absorption data for all investigated samples at various peak THz electric field strengths. We then use a fitting operation to relate these parameters to the nonlinear phase and extract the nonlinear indices. Extraction of the refractive index and absorption coefficient rely on conventional spectroscopy techniques [9,10]. The transfer function is found as the ratio of sample to reference fields in the frequency domain,

$$H(\omega) = \frac{\tau E_{\text{sam}}(\omega)}{E_{\text{ref}}(\omega)} \times \text{FP}(\omega). \qquad (1)$$

In Eq. (1), τ represents the Fresnel transmission coefficient while $\text{FP}(\omega)$ represents the Fabry–Perot effects [11]. In order to determine the index of refraction of the samples within the cell in an efficient manner, the index (linear and nonlinear) of the PLA material must first be determined. We print a test flat with thickness of 2 mm and use it as a sample. If a single sample is used, there is an external Fresnel transmission coefficient, an internal transmission coefficient, an external reflection, an internal reflection, and a Fabry–Perot term in Eq. (1). For the nonlinear measurements, the index of refraction is extracted at the focus for eight peak electric field values. The index and absorption coefficient are found through the relations by Eqs. (2) and (3):

$$\phi^T(\omega) = \frac{\omega L_{\text{sam}}}{c} [n_{\text{sam}}(\omega) - n_{\text{air}}(\omega)], \qquad (2)$$

and

$$\ln[|H(\omega)|]^T = -\frac{L_{\text{sam}}}{2} [\alpha_{\text{sam}}(\omega) - \alpha_{\text{air}}(\omega)]. \qquad (3)$$

Here, n_{sam} and L_{sam} are the sample index of refraction and the sample thickness, respectively. It is expected that n_{sam} and α_{sam} will vary slightly with increasing THz peak intensity caused by nonlinearity. The (T) superscript denotes that the operation is performed on the test flat (PLA material). The phase noise is accounted for and measured as the standard deviation across three averages for each peak electric field value probed. The index of refraction is defined as $n(\omega) = n^o(\omega) + n_2 I_{\text{THz}}$, where n^o denotes the linear portion, n_2 is the Kerr coefficient in m^2/W, and I_{THz} is the THz peak intensity in W/m^2 [12,13]. Similarly, $\alpha(\omega) = \alpha^o(\omega) + \alpha_2 I_{\text{THz}}$, where α^o is the linear absorption coefficient in m^{-1}, and α_2 denotes the two-photon absorption in meters per watt (m/W). The lowest intensity scan defines the linear dielectric constants, and the high electric field scans expose the trend of the index with respect to intensity.

Since the water vapor in our laboratory environment is not controlled, nor is it computationally removed, the nonlinear index of the samples cannot be decoupled from the nonlinear index of the water vapor, and we must instead represent the nonlinearity as a difference between the effects of the sample material and water vapor. In our model, water vapor is the main contributor to the nonlinearity in air (the reference material)

as the nitrogen, oxygen, and argon molecular modes cannot induce a nonlinear response [1]. As such, treating water vapor as the reference and applying the full definition of the index of refraction, Eqs. (2) and (3) lead to

$$\phi^T(\omega) = \frac{\omega L_{\text{sam}}}{c} [n_d^o(\omega) + n_{2,d}(\omega) I_{\text{THz}}], \qquad (4)$$

and

$$\ln[|H(\omega)|]^T = -\frac{L_{\text{sam}}}{2} [\alpha_d^o(\omega) + \alpha_{2,d}(\omega) I_{\text{THz}}], \qquad (5)$$

where $n_d^o(\omega) = n_{\text{sam}}^o(\omega) - n_{\text{air}}^o(\omega)$, $n_{2,d}(\omega) = n_{2,\text{sam}}(\omega) - n_{2,\text{air}}(\omega)$, and α parameters follow, respectively. A fit can then be done to Eqs. (4) and (5) to extract $n_{2,d}$ and $\alpha_{2,d}$ for every point along the THz frequency space.

A similar process is done for determining the index of the samples within the cells. Given that the PLA index is known for different peak electric fields, the sample can be treated as a three-layer structure. Here, n_{mat} now designates the known index of refraction of the PLA, while n_{sam} relates to the sample within the cell. There are now two internal reflection and transmission coefficients, two external reflection and transmission coefficients, and three Fabry–Perot terms to evaluate in Eq. (1). The dielectric constants are extracted as

$$n_{\text{sam}}(\omega) = \frac{\frac{c\phi^S(\omega)}{\omega} + n_{\text{air}}(\omega) L_{\text{eff}} - n_{\text{mat}}(\omega) [L_{\text{eff}} - L_{\text{sam}}]}{L_{\text{sam}}}, \qquad (6)$$

and

$$\alpha_{\text{sam}}(\omega) = \frac{-2\ln[|H(\omega)|]^s + \alpha_{\text{air}}(\omega) L_{\text{eff}} - \alpha_{\text{mat}}(\omega) [L_{\text{eff}} - L_{\text{sam}}]}{L_{\text{sam}}}. \qquad (7)$$

Above, L_{eff} is the total propagation length of the THz beam. Albeit more complicated, we see that Eqs. (6) and (7) reduce to Eqs. (2) and (3) in the limit that $L_{\text{eff}} = L_{\text{sam}}$. The (S) superscript denotes operation on the sample. As done previously, the low power scan denotes the linear operation, while the ensuing high-power scans elucidate on the nonlinear behavior. The full phase is represented as

$$\Delta\phi(\omega) = \frac{\omega}{c} \big[(n_d^o(\omega) + n_{2,d}(\omega) I_{\text{THz}}) L_{\text{eff}}$$
$$+ (n_k^o(\omega) + n_{2,k}(\omega) I_{\text{THz}}) L_{\text{sam}} \big], \qquad (8)$$

and the magnitude shift is represented as

$$\Delta ln [|H(\omega)|] = -\frac{1}{2} \big[(\alpha^o(\omega) + \alpha_{2,d}(\omega) I_{\text{THz}}) L_{\text{eff}}$$
$$+ (\alpha_k^o(\omega) + \alpha_{2,k}(\omega) I_{\text{THz}}) L_{\text{sam}} \big]. \qquad (9)$$

A fit to Eqs. (8) and (9) solves for the value of $n_{2,k}(\omega) = n_{2,\text{sam}}(\omega) - n_{2,\text{mat}}(\omega)$. Finally, addition between $n_{2,d}$ and $n_{2,k}$ leads to $\Delta n_2 = n_{2,\text{sam}} - n_{2,\text{air}}$. Note that $n_k^o(\omega) = n_{\text{sam}}^o(\omega) - n_{\text{mat}}^o(\omega)$ and α follows, respectively.

An analysis along the detectable bandwidth is made for liquid water, α-pinene, and Si. Figure 1(a) plots the fit to the full phase in Eq. (8) versus peak intensity for all three materials and the PLA material at 0.5 THz. In the presence of nonlinearity, the fit is a straight line with a slope proportional to the value of Δn_2. A non-zero slope indicates that there is nonlinear action
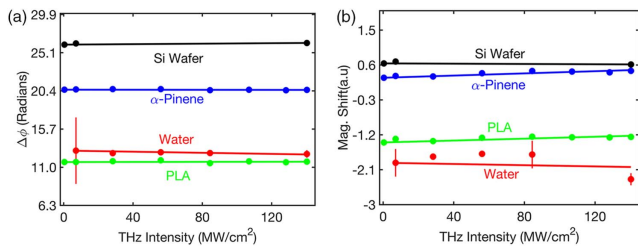
Fig. 1. Fitting lines performed in accordance to phase and magnitude equations for all tested materials at 0.5 THz. (a) Fit to Eq. (8) versus peak intensity shows good agreement with data. Error bars indicate phase noise error. (b) Fitting lines to Eq. (9) with respect to intensity. Error bars indicate standard deviations in the magnitude of the transfer function. The liquid water shows deviation in the magnitude due to high absorption.

present. Figure 1(b) showcases the magnitude shift as a fit for Eq. (9) versus peak intensity for all materials at 0.5 THz. The deviation of the liquid water magnitude in Fig. 1(b) is due to the strong absorption from the water sample, while the high error on the first point of the liquid water phase fit in Fig. 1(a) is due to phase noise errors. The error bars indicate the phase noise and fluctuation of the magnitude values. The phase noise is large because the liquid water attenuation is high, and the sample is relatively thin. Additionally, the collection optics after the sample position vignette some of the THz beam, further reducing the collected THz energy. Aside from these points, extracted phases and magnitudes agree very well with their fits and showcase that the values are nominally above the phase and magnitude noise. However, as can be seen, the fluctuations themselves do not follow a perfectly linear trend, although they do collectively tend toward a straight line. The oscillation about the linear fit is due to stage error.

The application of this analysis for every point in the frequency along the detectable bandwidth (0.3–1.1 THz) for all materials yields the dispersion of Δn_2 and $\Delta \alpha_2$ in the samples. The dispersion of Δn_2 for the PLA material is shown in Fig. 2. The plot shows clear resonances corresponding to known spectral features for water vapor at 0.4, 0.56, 0.74, and 1.10 THz [14]. Because the orders of magnitude of the PLA n_2 and water vapor n_2 are expected to be the same, spectrally resolved Kerr coefficients are difficult to extract. Additionally, Fig. 2 shows that as the nonlinear index changes its sign the absorption reaches a peak value. This is consistent with the expected behavior from the Lorentz oscillator model [12]. Extension of the measurement window and a reduction of our time constant will
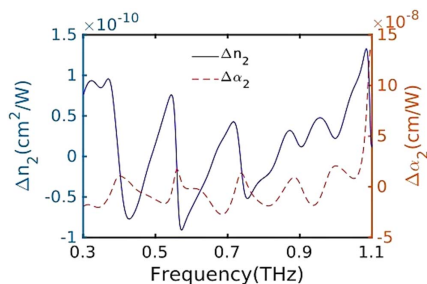

Fig. 2. Dispersion of the calculated nonlinear index difference as a result of applying Eqs. (2) and (3) for every point along the detectable frequency of PLA. The peaks coincide with known resonances for water vapor at 0.4, 0.56, 0.74, and 1.10 THz.

allow for a spectrally resolved demonstration of n_2 and α_2 in the THz range.

All samples are treated as non-centrosymmetric in our analysis based on their lack of molecular point symmetry. As such, the nonlinear absorption resonances can coincide with the linear resonances. According to the model presented in Ref. [1], while the main driving nonlinear process in the optical regime is governed by the electronic response of the third-order susceptibility, it is theorized that the THz response is driven by molecular nonlinearities—that is to say, due to the rotational and vibrational modes of a molecule. Moreover, the presence of sharp absorption peaks for many materials in the THz regime allows for large values of n_2 given that the nonlinearity is expressed as a combination of off-resonant and resonant responses.

In the specific case of the PLA material, no sharp resonances were found in the linear regime evaluation, but the contribution of water vapor could not be decoupled from the contribution of the PLA. Fortunately, the differences between the PLA and water vapor n_2 as well as between the sample and PLA n_2 are more important for determining the pure sample n_2. While the water vapor prevented a spectrally resolved measurement of n_2 and α_2, spectral averaging upon the detectable bandwidth can be done, and estimated values for the Kerr coefficients could be found. First, we acknowledge that Si is effectively a centrosymmetric molecule but may exhibit a non-centrosymmetric response due to its surface, as is found in the optical regime. This effect would be very small and difficult to detect with our system. In our experiment, the peak intensity used to test Si is $140 \, \text{MW/cm}^2$. The mean change to the index observed is $\Delta n = n_2 I = +0.008$. This sets a lower limit of detection for n_2 as $10^{-11} \, \text{cm}^2/\text{W}$. Fortunately, the spectrally averaged value of Si has been evaluated before and found to be one order lower [15]. As such, the Δn_2 found in our experiment completely describes the spectrally averaged value of water vapor as $6 \times 10^{-11} \, \text{cm}^2/\text{W}$. This value is in line with observations presented in Ref. [16].

Using this value as the mean reference and evaluating the mean nonlinear index differences, we can extract nonlinear index data for all other samples. The extracted values are listed in Table 1. The spectrally averaged values are shown for n_2 and α_2 along 0.3–1.1 THz. The maximum THz peak intensity used is $140 \, \text{MW/cm}^2$, and the minimum peak intensity is $0.4 \, \text{MW/cm}^2$. Linear refractive index values are shown for 0.9 THz and gathered at the lowest peak electric field. We anticipate that without eliminating the water vapor altogether, spectrally resolved Kerr coefficients cannot be easily extracted, as known vapor resonances along 0.40, 0.56, 0.74, and 1.10 THz can cause considerable fluctuations [14]. These resonances also appear in the dispersion of Δn_2, as shown in Fig. 2.

Considering the model presented in Ref. [1], n_2 for liquid water can be as large as $7 \times 10^{-10} \, \text{cm}^2/\text{W}$ [4]. In our method, unlike the vapor phase, liquid water does not have sharp resonances within our detectable bandwidth. This means that the nonlinear coefficients are not expected to switch signs. With a peak intensity of $140 \, \text{MW/cm}^2$ and a mean phase noise leading to $\Delta n_{\text{noise}} = +0.04$, liquid water has an approximate n_2 of $7.8 \pm 3 \times 10^{-10} \, \text{cm}^2/\text{W}$. The high error is expected, as the attenuation is strong in liquid water. Fortunately, the value is within the expected range. Lastly, α-pinene has very negligible absorption and dispersion along the linear regime, and α-pinene can best be identified as having a

Table 1. Extracted Kerr Coefficients

Sample	n	α (cm^{-1})	n_2 (cm^2/W)	α_2 (cm/W)
Si	3.41	20	—	—
H$_2$O Vapor	—	—	0.6×10^{-10}	-2.0×10^{-10}
Liquid H$_2$O	2.33	230	$7.8 \pm 3 \times 10^{-10}$	-2.0×10^{-10}
α-pinene	1.66	1.5	$1.3 \pm 0.01 \times 10^{-10}$	$-2.4 \pm 0.05 \times 10^{-10}$

C_1 point group molecular structure [17]. With our method, with a peak intensity of 140 MW/cm^2 and a mean phase noise leading to $\Delta n_{\text{noise}} = +0.0002$, α-pinene has an n_2 of $1.30 \pm 0.01 \times 10^{-10}$ cm^2/W.

A flip in the sign for all samples was enacted via a phenomenological approach since physically, according to the model in Ref. [1], the mean Kerr coefficients for noncentrosymmetric samples are generally positive. A similar treatment for the nonlinear absorption reveals that α_2 produces mean values of -2.0×10^{-10} cm/W for water vapor, $-4.4 \pm 0.2 \times 10^{-10}$ cm/W for liquid water, and $-2.40 \pm 0.05 \times 10^{-10}$ cm/W for α-pinene. These numbers indicate a mostly dominant saturable absorption process in all three samples. Specifically, for water, this observation was also seen in the Z-scan curves in Ref. [4]. The above result is interesting because it implies that a dynamic gain process may be possible for THz pulses inside the materials under strong peak fields (>3 MV/cm). However, it is also possible that the contributions from the higher-order odd nonlinearities may offset the reduction of the losses at high intensity. More detailed studies regarding spectrally resolved measurements will be required to confirm these claims. Moreover, our current results suggest that significant changes in the index of refraction are possible with viably reachable peak electric field strengths. For example, in the case of α-pinene, the linear index of refraction is 1.66, and a peak THz electric field of 2.2 MV/cm would induce a nonlinear index shift $\Delta n = 1.66$. At higher peak electric fields, the perturbative model for the nonlinear susceptibility is broken, and a new formulation for the nonlinear index of refraction and nonlinear absorption must be considered. In such a regime, it is possible for the nonlinear index and nonlinear absorption to quickly saturate. This is important, as it indicates that non-perturbative nonlinear optics can be studied in the THz regime without invoking relativistic laser intensities. It is worth noting that the fluctuations shown about the fit for Fig. 1 may also indicate that a nonlinear saturation point may have been reached. Further studies regarding this topic will be conducted in the future.

In closing, we experimentally demonstrate the spectrally averaged nonlinear Kerr coefficients for three samples (water, α-pinene, and Si) and water vapor along the spectral region between 0.3 to 1.1 THz. The work takes advantage of the fact that THz-TDS allows for a full-phase analysis, leading to direct methods of extracting nonlinear parameters from an experiment. The results show agreement with Z-scan techniques and are advantageous in that the beam mode need not be pre-specified. Furthermore, we plan to conduct these experiments in a humidity-controlled environment in order to fully and properly deduce the nonlinear coefficients in a spectrally resolved measurement. Future experiments will also focus on the study of the non-perturbative nonlinear optics in THz frequencies, where relativistic laser intensities are not required.

Disclosures. The authors declare no conflicts of interest.

REFERENCES

1. K. Dolgaleva, D. V. Materikina, R. W. Boyd, and S. A. Kozlov, Phys. Rev. A **92**, 023809 (2015).
2. A. N. Tcypkin, S. E. Putilin, M. S. Kulya, and S. Choudhary, *42nd International Conference on Infrared, Millimeter, and Terahertz Waves (IRMMW-THz)* (2017), Vol. **1588**, pp. 265–270.
3. S. A. Stumpf, A. A. Korolev, and S. A. Kozlov, Proc. SPIE **6614**, 661408 (2007).
4. A. N. Tcypkin, M. V. Melnik, M. O. Zhukova, I. O. Vorontsova, S. E. Putilin, S. A. Kozlov, and X.-C. Zhang, Opt. Express **27**, 10419 (2019).
5. P. Kabaciński, T. M. Kardaś, Y. Stepanenko, and C. Radzewicz, Opt. Express **27**, 11018 (2019).
6. D. J. Cook and R. M. Hochstrasser, Opt. Lett. **25**, 1210 (2000).
7. K. Y. Kim, Phys. Plasmas **16**, 056706 (2009).
8. Q. Wu and X. C. Zhang, Appl. Phys. Lett. **67**, 3523 (1995).
9. W. Withayachumnankul, B. Ferguson, T. Rainsford, S. P. Mickan, and D. Abbott, Proc. SPIE **5840**, 221 (2005).
10. P. U. Jepsen, J. Infrared Millim. Terahertz Waves **40**, 395 (2019).
11. J. Neu and C. A. Schmuttenmaer, J. Appl. Phys. **124**, 231101 (2018).
12. R. W. Boyd, *Nonlinear Optics*, 3rd ed. (Academic, 2008).
13. G. Agrawal, *Nonlinear Fiber Optics*, 5th ed. (Elsevier, 2012).
14. R. J. Foltynowicz and R. E. Allman, "Terahertz time-domain spectroscopy of atmospheric water vapor from 0.4 to 2.7 THz," Technical Report AC04-94AL85000 (2005).
15. A. Woldegeorgis, T. Kurihara, B. Beleites, J. Bossert, R. Grosse, G. G. Paulus, F. Ronneberger, and A. Gopal, J. Infrared Millim. Terahertz Waves **39**, 667 (2018).
16. P. Rasekh, M. Yildirim, A. Safari, J.-M. Ménard, R. Bhardwaj, K. Dolgaleva, and R. W. Boyd, Proc. SPIE **11264**, 112640P (2020).
17. H. William Wilson, Appl. Spectrosc. **30**, 209 (1976).